Fractional Tikhonov regularization with a nonlinear penalty term

FRACTIONAL TIKHONOV REGULARIZATION WITH A NONLINEAR PENALTY TERM

SERENA MORIGI*, LOTHAR REICHEL†, AND FIORELLA SGALLARI‡

Abstract. Tikhonov regularization is one of the most popular methods for solving linear systems of equations or linear least-squares problems with a severely ill-conditioned matrix and an error-contaminated data vector (right-hand side). This regularization method replaces the given problem by a penalized least-squares problem. It is well known that Tikhonov regularization in standard form may yield approximate solutions that are too smooth, i.e., the computed approximate solution may lack many details that the desired solution of the associated, but unavailable, error-free problem might possess. Fractional Tikhonov regularization methods have been introduced to remedy this shortcoming. However, the computed solution determined by fractional Tikhonov methods in standard form may display undesirable spurious oscillations. This paper proposes that fractional Tikhonov methods be equipped with a nonlinear penalty term, such as a TV-norm penalty term, to reduce unwanted oscillations. Numerical examples illustrate the benefits of this approach.

1. Introduction. We are concerned with the approximate solution of linear least-squares problems

$$\min_{\boldsymbol{x}\in\mathbb{R}^n} \|A\boldsymbol{x}-\boldsymbol{b}\|_2 \tag{1.1}$$

with a matrix $A \in \mathbb{R}^{m\times n}$ that has many singular values of different orders of magnitude close to the origin; some singular values may vanish. Least-squares problems with a matrix of this kind are often referred to as discrete ill-posed problems. For notational convenience, we will assume that $m \geq n$; however, the methods discussed also can be applied when $m < n$. The situation when $m = n$ is of particular interest. Then (1.1) simplifies to a linear system of equations that may be inconsistent.

The vector $\boldsymbol{b} \in \mathbb{R}^m$ in (1.1) represents available data, which are contaminated by an error $\boldsymbol{e} \in \mathbb{R}^m$ that stems from measurement inaccuracies. Thus,

$$\boldsymbol{b} = \widehat{\boldsymbol{b}} + \boldsymbol{e}, \tag{1.2}$$

where $\widehat{\boldsymbol{b}}$ is the unknown error-free vector associated with $\boldsymbol{b}$. The unavailable linear system with error-free right-hand side,

$$A\boldsymbol{x} = \widehat{\boldsymbol{b}}, \tag{1.3}$$

is assumed to be consistent. This allows us to apply the discrepancy principle to determine the regularization parameter in Tikhonov regularization; see below.

Let $\widehat{\boldsymbol{x}}$ denote the solution of (1.3) of minimal Euclidean norm. We would like to determine an approximation of $\widehat{\boldsymbol{x}}$ by computing a suitable approximate solution of (1.1). Due to the error $\boldsymbol{e}$ in $\boldsymbol{b}$ and the fact that the singular values of A "cluster" at the origin, the solution of minimal Euclidean norm of (1.1) typically is a poor approximation of $\widehat{\boldsymbol{x}}$.

*Department of Mathematics, University of Bologna, Bologna, Italy.
E-mail: serena.morigi@unibo.it
†Department of Mathematical Sciences, Kent State University, Kent, OH 44242, USA.
E-mail: reichel@math.kent.edu
‡Department of Mathematics, University of Bologna, Bologna, Italy.
E-mail: fiorella.sgallari@unibo.it

Tikhonov regularization is a popular approach to determine an approximation of $\widehat{\boldsymbol{x}}$. This method replaces the minimization problem (1.1) by a penalized least-squares problem. Tikhonov regularization in standard form replaces (1.1) by

$$\min_{\boldsymbol{x}\in\mathbb{R}^n}\{\|A\boldsymbol{x}-\boldsymbol{b}\|_2^2+\mu\,\|\boldsymbol{x}\|_2^2\}. \tag{1.4}$$

Throughout this paper $\|\cdot\|_2$ denotes the Euclidean vector norm or the spectral matrix norm. The scalar $\mu\geq 0$ is referred to as a regularization parameter. The Tikhonov minimization problem (1.4) has the unique solution

$$\boldsymbol{x}_\mu=(A^TA+\mu I)^{-1}A^T\boldsymbol{b} \tag{1.5}$$

for any fixed $\mu>0$. Here the superscript ^{T} denotes transposition. The value of $\mu>0$ determines how sensitive the Tikhonov solution $\boldsymbol{x}_\mu$ is to the error $\boldsymbol{e}$ in $\boldsymbol{b}$, and how close $\boldsymbol{x}_\mu$ is to the desired vector $\widehat{\boldsymbol{x}}$. The determination of a suitable value of μ is an important part of the solution process. In most of the computed examples in Section 4, we determine μ by the discrepancy principle. However, the regularization methods proposed in this paper also can be applied together with other schemes for determining the regularization parameter, such as the L-curve criterion and generalized cross validation; see [10, 15, 23] for discussions on and computed examples with many methods for determining the regularization parameter in (1.4).

The approximation $\boldsymbol{x}_\mu$ of $\widehat{\boldsymbol{x}}$ obtained with Tikhonov regularization is known to generally be too smooth, i.e., $\boldsymbol{x}_\mu$ typically lacks many details that $\widehat{\boldsymbol{x}}$ may have; see, e.g., Hansen [10, p. 180] for a discussion and references. A reason for this is that the available data vector $\boldsymbol{b}$ is multiplied by A^T in (1.5). In applications of interest to us, the matrix A^T is a low-pass filter, such as a blurring matrix, and fine details that may be present in $\boldsymbol{b}$ are smoothed when forming $A^T\boldsymbol{b}$. These details therefore are difficult or impossible to recover.

Two variants of Tikhonov regularization (1.4), both referred to as *fractional Tikhonov methods*, have been proposed in the literature to reduce the over-smoothing obtained with Tikhonov regularization (1.4); see [13, 16]. The method discussed in [13] replaces the minimization problem (1.4) by the weighted least-squares problem

$$\min_{\boldsymbol{x}\in\mathbb{R}^n}\{\|A\boldsymbol{x}-\boldsymbol{b}\|_W^2+\mu\,\|\boldsymbol{x}\|_2^2\}, \tag{1.6}$$

where $\|\boldsymbol{x}\|_W=(\boldsymbol{x}^TW\boldsymbol{x})^{1/2}$ and

$$W=(AA^T)^{(\alpha-1)/2} \tag{1.7}$$

for a suitable value of $\alpha>0$. We are primarily interested in $0<\alpha<1$; for $\alpha=1$, the minimization problem (1.6) simplifies to (1.4). The theory developed in [8] is for $-1<\alpha<1$. We define W with the aid of the Moore–Penrose pseudoinverse of A when $\alpha<1$. We note for future reference that the normal equations associated with the minimization problem (1.6) are of the form

$$((A^TA)^{(\alpha+1)/2}+\mu\,I)\boldsymbol{x}=(A^TA)^{(\alpha-1)/2}A^T\boldsymbol{b}. \tag{1.8}$$

Introduce the singular value decomposition (SVD) of A,

$$A=U\Sigma V^T, \tag{1.9}$$

where $U = [\boldsymbol{u}_1, \boldsymbol{u}_2, \ldots, \boldsymbol{u}_m] \in \mathbb{R}^{m\times m}$ and $V = [\boldsymbol{v}_1, \boldsymbol{v}_2, \ldots, \boldsymbol{v}_n] \in \mathbb{R}^{n\times n}$ are orthogonal matrices, and

$$\Sigma = \mathrm{diag}[\sigma_1, \sigma_2, \ldots, \sigma_n] \in \mathbb{R}^{m\times n}.$$

The singular values are ordered according to

$$\sigma_1 \geq \sigma_2 \geq \ldots \geq \sigma_r > \sigma_{r+1} = \ldots = \sigma_n = 0,$$

where the index r is the rank of A; see, e.g., [3, 9] for discussions on properties and the computation of the SVD. We will assume that A is scaled so that

$$\sigma_1 = \|A\|_2 < 1. \tag{1.10}$$

Substituting the SVD of A into the right-hand side of (1.8) yields

$$(A^TA)^{(\alpha-1)/2}A^T\boldsymbol{b} = V\widetilde{S}_1^{\alpha}U^T\boldsymbol{b}, \tag{1.11}$$

where $\widetilde{S}_1^{\alpha} = \mathrm{diag}[\sigma_1^{\alpha}, \sigma_2^{\alpha}, \ldots, \sigma_r^{\alpha}, 0, \ldots, 0] \in \mathbb{R}^{n\times m}$. When $0 < \alpha < 1$, the components $(U^T\boldsymbol{b})_j$, $j = 1, 2, \ldots, m$, of the vector $U^T\boldsymbol{b}$ are damped; they are damped more for large values of j than for small values. The damping decreases as α decreases. The reduced damping for $\alpha < 1$, compared with $\alpha = 1$, is the main reason for the reduced smoothing obtained when solving (1.6) instead of (1.4). The seminorm $\|\cdot\|_W$ in (1.6) allows the parameter α to be chosen to improve the quality of the solution

$$\boldsymbol{x}_{\mu,\alpha} = ((A^TA)^{(\alpha+1)/2} + \mu I)^{-1}(A^TA)^{(\alpha-1)/2}A^T\boldsymbol{b} \tag{1.12}$$

of (1.6). A detailed discussion of the smoothing properties of the method (1.6) in terms of filter factors is provided in [13].

In numerous computed examples reported in [13], the inequality

$$\|\boldsymbol{x}_{\mu_\alpha,\alpha} - \widehat{\boldsymbol{x}}\|_2 < \|\boldsymbol{x}_{\mu} - \widehat{\boldsymbol{x}}\|_2 \tag{1.13}$$

holds when α is a positive constant smaller than unity and the regularization parameters μ in (1.4) and $\mu = \mu_\alpha$ in (1.6) are determined by the discrepancy principle. However, computed examples reported in [8] show that for many problems the solutions $\boldsymbol{x}_{\mu_\alpha,\alpha}$ of (1.6) for some $0 < \alpha < 1$ are more oscillatory than the corresponding solutions $\boldsymbol{x}_{\mu}$ of (1.4). It is therefore not clear whether the former solutions are more useful in applications than the latter, even when the inequality (1.13) holds. The analysis in [8] shows that when the singular values of A decrease to zero quickly with increasing index, or when the error $\boldsymbol{e}$ is dominated by low-frequency noise, the solution $\boldsymbol{x}_{\mu_\alpha,\alpha}$ of (1.6) generally is a more useful approximation of $\widehat{\boldsymbol{x}}$ than the corresponding solution $\boldsymbol{x}_{\mu}$ of (1.4). This is confirmed by computed examples reported in [8].

It is the purpose of the present paper to seek to increase the set of linear discrete ill-posed problems (1.1) for which it is advantageous to use fractional Tikhonov regularization by modifying the penalty function $\|\boldsymbol{x}\|_2^2$ in (1.6). We propose that the ℓ_2-norm be replaced by a suitable nonlinear function to reduce spurious oscillations in the computed solution. For instance, we consider the use of TV-norm regularization

$$\min_{\boldsymbol{x}\in\mathbb{R}^n}\{\|A\boldsymbol{x} - \boldsymbol{b}\|_W^2 + \mu\,\|\boldsymbol{x}\|_{\mathrm{TV}}\}. \tag{1.14}$$

When $\boldsymbol{x} \in \mathbb{R}^n$ represents a signal in one space-dimensions, we have

$$\|\boldsymbol{x}\|_{\mathrm{TV}} = \sum_{i=1}^{n} |(D\boldsymbol{x})_i|,$$

where the operator D is a finite difference approximation of the first-order derivative and $(D\boldsymbol{x})_i$ denotes the ith component of the vector $D\boldsymbol{x}$. The TV-norm is defined analogously for signals in higher space-dimensions; see Section 4. Penalty functions of the form

$$\|D\boldsymbol{x}\|_q^q = \sum_{i=1}^{n} |(D\boldsymbol{x})_i|^q, \qquad \boldsymbol{x} = [x_1, x_2, \ldots, x_n]^T, \tag{1.15}$$

for some $0 < q < 2$ also will be considered. An automatic strategy for the choice of the parameter q for image restoration problems is provided in [18]. Computed examples in [6, 17, 18] show ℓ_q-quasi-norm ($q < 1$) regularization to yield more accurate image restorations than ℓ_1-norm regularization. This is due to the fact that the ℓ_q-quasi-norm gives sparser restorations and better preserves edges than the ℓ_1-norm.

This paper is organized as follows. Section 2 reviews properties of the solution $\boldsymbol{x}_{\mu,\alpha}$ of (1.6) as functions of $\alpha \geq 0$ and $\mu > 0$. Some new results for the situation when the term $\mu \|\boldsymbol{x}\|_2^2$ in (1.6) is replaced by $\mu \|L\boldsymbol{x}\|_2^2$ for some special matrices L are shown. These minimization problems are simpler to analyze than the problem (1.14). Nevertheless, results for the simpler problems shed some light on the problem (1.14). Section 3 discusses how the computations for fractional Tikhonov regularization can be carried out, both for small and large-scale problems. A few computed examples that illustrate the advantages of choosing $\alpha > 0$ in (1.14) are presented in Section 4, and concluding remarks can be found in Section 5.

We conclude this section with some comments on the available literature on fractional Tikhonov regularization methods. These methods were probably first described by Louis [19] and have subsequently been analyzed by Mathé and Tautenhahn [20]. Properties of fractional Tikhonov regularization also are discussed in [13]. Computed examples in [13] show that approximations of the desired vector $\widehat{\boldsymbol{x}}$ determined by fractional Tikhonov regularization (1.6) compare well with approximations of $\widehat{\boldsymbol{x}}$ computed by standard Tikhonov regularization (1.4) in the sense that the inequality (1.13) holds for many problems and values of $0 < \alpha < 1$. A recent review of the literature with new theoretical results and further computed examples are presented in [8]. Fractional Lavrentiev regularization for linear discrete ill-posed problems (1.1) with a square positive semidefinite matrix A is discussed in [12, 21]. Iterated fractional Tikhonov regularization has recently been described by Bianchi et al. [2].

Klann and Ramlau [16] proposed an approach different from (1.6) to reduce the over-smoothing of standard Tikhonov regularization. They compute

$$\boldsymbol{x}_{\mu,\gamma} = (A^TA + \mu I)^{-\gamma}(A^TA)^{(\gamma-1)}A^T\boldsymbol{b}$$

for some $\gamma > 1/2$ and also refer to their scheme as a fractional Tikhonov method. The vector $\boldsymbol{x}_{\mu,\gamma}$ simplifies to (1.5) when $\gamma = 1$. For $\gamma \neq 1$, $\boldsymbol{x}_{\mu,\gamma}$ is not the solution of a minimization problem of the form (1.6). The fractional Tikhonov method by Klann and Ramlau [16] therefore does not naturally fit into the framework of the present paper. Its properties are also investigated in [8].

2. Some properties of fractional Tikhonov regularization. Assume that a fairly accurate bound, δ, for the error in $\boldsymbol{b}$ is known, i.e.,

$$\|\boldsymbol{e}\|_2 \leq \delta. \tag{2.1}$$

The discrepancy principle applied to the solution of (1.6) prescribes that for a fixed $\alpha \geq 0$, the regularization parameter $\mu = \mu_\alpha$ be chosen so that the solution (1.12)

satisfies

$$\|A\boldsymbol{x}_{\mu,\alpha} - \boldsymbol{b}\|_2 = \eta\delta. \tag{2.2}$$

Here $\eta > 1$ is a fixed parameter that is independent of δ. Gerth et al. [8] show in a Hilbert space setting that this approach to determine $\mu = \mu_\alpha$ defines an order optimal regularization method; in particular $\lim_{\delta\searrow 0} \boldsymbol{x}_{\mu_\alpha,\alpha} = \widehat{\boldsymbol{x}}$.

Computed examples reported in [8] show that the choice of η may affect the performance of the standard and fractional Tikhonov regularization methods (1.4) and (1.6), respectively, and that standard Tikhonov regularization typically performs the best when $\eta = 1$. We therefore set $\eta = 1$ in the remainder of this paper unless explicitly stated otherwise.

The value of μ such that the solution $\boldsymbol{x}_{\mu,\alpha}$ of (1.6) satisfies (2.2) for a fixed $0 < \alpha \leq 1$ depends on δ. It is shown in [13, Proposition 3.1] that $d\mu/d\delta > 0$, i.e., an error $\boldsymbol{e}$ in $\boldsymbol{b}$ of large norm requires $\mu = \mu_\alpha$ to be larger than an error of small norm. It follows from the expression (1.12) that $\|\boldsymbol{x}_{\mu,\alpha}\|_2$ decreases as $\mu > 0$ increases for fixed α. We therefore can expect $\|\boldsymbol{x}_{\mu,\alpha}\|_2$ to be smaller than $\|\widehat{\boldsymbol{x}}\|_2$. In particular, when δ is large, $\|\boldsymbol{x}_{\mu,\alpha}\|_2$ might be much smaller than $\|\widehat{\boldsymbol{x}}\|_2$. We will, under special conditions, show that $d\mu_\alpha/d\alpha \geq 0$. It follows that decreasing α from one reduces $\mu = \mu_\alpha$ and, therefore, increases $\|\boldsymbol{x}_{\mu,\alpha}\|_2$. We remark that the solution $\mu = \mu_\alpha$ of (2.2) for fixed α can be determined by a zero-finder; see [8, 13] for details.

The minimization problem (1.14) or the minimization problem with the TV-norm penalty term replaced by (1.15) can be solved by iteratively reweighted norm methods; see, e.g., [14, 17, 24]. These methods compute the desired solution by solving a sequence of weighted least-squares problems. Each one of these problems can be written as (1.4) with the penalty function $\|\boldsymbol{x}\|_2^2$ replaced by a function of the form $\|L\boldsymbol{x}\|_2^2$ with a matrix $L \in \mathbb{R}^{p\times n}$. We therefore are interested in investigating the behavior of the solution $\boldsymbol{x}_{\mu,\alpha}$ of minimization problems of the form

$$\min_{\boldsymbol{x}\in\mathbb{R}^n} \{\|A\boldsymbol{x} - \boldsymbol{g}\|_W^2 + \mu \|L\boldsymbol{x}\|_2^2\}. \tag{2.3}$$

Let $\mathcal{N}(M)$ denote the null space of the matrix M. We will assume that

$$\mathcal{N}(A) \cap \mathcal{N}(L) = \{\boldsymbol{0}\}. \tag{2.4}$$

Then the minimization problem (2.3) has a unique solution $\boldsymbol{x}_{\mu,\alpha}$ for any $\mu > 0$ and $0 < \alpha < 1$.

We first study the behavior of $\mu \to \boldsymbol{x}_{\mu,\alpha}$ for fixed $0 < \alpha \leq 1$. The matrix L is not required to be of full rank. We assume for notational simplicity that $m \geq n \geq p$, but this restriction can be removed; see below. It is convenient to use the generalized singular value decomposition (GSVD) of the matrix pair $\{W^{1/2}A, L\}$. It is given by

$$W^{1/2}A = W_1 S_1 X^T, \qquad L = W_2 S_2 X^T, \tag{2.5}$$

where the matrices $W_1 \in \mathbb{R}^{m\times m}$ and $W_2 \in \mathbb{R}^{p\times p}$ are orthogonal,

$$S_1 = \mathrm{diag}[s_1^{(1)}, s_2^{(1)}, \ldots, s_n^{(1)}] \in \mathbb{R}^{m\times n}, \qquad S_2 = \mathrm{diag}[s_1^{(2)}, s_2^{(2)}, \ldots, s_p^{(2)}] \in \mathbb{R}^{p\times n},$$

and $X \in \mathbb{R}^{n\times n}$ is nonsingular. The nontrivial entries of S_1 and S_2 satisfy

$$0 \leq s_1^{(1)} \leq s_2^{(1)} \leq \ldots s_n^{(1)} \leq 1, \qquad 1 \geq s_1^{(2)} \geq s_2^{(2)} \geq \ldots \geq s_p^{(2)} \geq 0$$

with

$$\left(s_i^{(1)}\right)^2 + \left(s_i^{(2)}\right)^2 = 1, \qquad 1 \le i \le p,$$

and $s_{p+1}^{(1)} = \ldots = s_n^{(1)} = 1$; see, e.g., [1, 3, 9] for details.

Let $\boldsymbol{w} = [w_1, w_2, \ldots, w_n]^T \in \mathbb{R}^n$. We will use the notation

$$(\boldsymbol{w})_{i:j} = [w_i, w_{i+1}, \ldots, w_j]^T \in \mathbb{R}^{j-i+1}$$

for subvectors. We remark that the GSVD of the matrix pair $\{W^{1/2}A, L\}$ is only used in our analysis; it is not required by the numerical methods used for the computed examples of this paper.

PROPOSITION 2.1. *Assume that* (2.4) *holds and let* $\boldsymbol{x}_\mu$ *denote the solution of* (2.3). *Let* $m \ge n \ge p$. *Then* $\|\boldsymbol{x}_\mu\|_2$ *decreases as* $\mu > 0$ *increases. When* $n = p$ *and* $s_p^{(2)} > 0$, *we have* $\lim_{\mu\to\infty} \|\boldsymbol{x}_\mu\|_2 = 0$. *More generally, with* $n \ge p$ *and* $s_k^{(2)} > s_{k+1}^{(2)} = \ldots = s_p^{(2)} = 0$, *it holds*

$$\lim_{\mu\to\infty} \|\boldsymbol{x}_\mu\|_2 = \left\| X^{-T} \begin{bmatrix} \mathbf{0} \\ (U_1^T W^{1/2} \boldsymbol{b})_{k+1:n} \end{bmatrix} \right\|_2. \tag{2.6}$$

Proof. The requirement (2.4) secures that the minimization problem (2.3) has a unique solution $\boldsymbol{x}_\mu$ for any $\mu > 0$. The normal equations associated with (2.3) are given by

$$(A^T W A + \mu\, L^T L)\boldsymbol{x} = A^T W \boldsymbol{b}. \tag{2.7}$$

Substituting (2.5) into (2.7) yields

$$(S_1^T S_1 + \mu\, S_2^T S_2)\boldsymbol{z} = S_1^T U_1^T W^{1/2} \boldsymbol{b}, \tag{2.8}$$

whose solution $\boldsymbol{z}_\mu$ determines the solution $\boldsymbol{x}_\mu = X^{-T}\boldsymbol{z}_\mu$ of (2.3). It follows from (2.8) that

$$\|\boldsymbol{z}_\mu\|_2^2 = \boldsymbol{b}^T W^{1/2} U_1 S_1 (S_1^T S_1 + \mu\, S_2^T S_2)^{-2} S_1^T U_1^T W^{1/2} \boldsymbol{b} \tag{2.9}$$

and, hence,

$$\frac{d}{d\mu}\|\boldsymbol{z}_\mu\|_2^2 = -2\boldsymbol{b}^T W^{1/2} U_1 S_1 (S_1^T S_1 + \mu\, S_2^T S_2)^{-3} S_2^T S_2 S_1^T U_1^T W^{1/2} \boldsymbol{b}.$$

Thus, $\frac{d}{d\mu}\|\boldsymbol{z}_\mu\|_2 \le 0$. The fact that $\frac{d}{d\mu}\|\boldsymbol{x}_\mu\|_2 \le 0$ follows similarly from the expression

$$\|\boldsymbol{x}_\mu\|_2^2 = \boldsymbol{b}^T W^{1/2} U_1 S_1 (S_1^T S_1 + \mu\, S_2^T S_2)^{-1} X^{-1} X^{-T} (S_1^T S_1 + \mu\, S_2^T S_2)^{-1} S_1^T U_1^T W^{1/2} \boldsymbol{b}.$$

Assume for the moment that $p = n$ and $s_n^{(2)} > 0$. Then (2.9) shows that $\|\boldsymbol{z}_\mu\| \to 0$, and therefore $\|\boldsymbol{x}_\mu\| \to 0$, as $\mu \to \infty$. More generally, let $n \ge p$ and assume that $s_k^{(2)} > s_{k+1}^{(2)} = \ldots = s_p^{(2)} = 0$. Then it follows from (2.8) that

$$\lim_{\mu\to\infty} \boldsymbol{z}_\mu = \begin{bmatrix} \mathbf{0} \\ (U_1^T W^{1/2} \boldsymbol{b})_{k+1:n} \end{bmatrix}.$$

This shows (2.6). ∎

The GSVD also can be defined for the matrix pair $\{W^{1/2}A, L\}$ when A has more columns than rows or L has more rows than A; see, e.g., [1, 3, 9]. Results analogous to Proposition 2.1 can be shown also for these situations.

We will next discuss how $\|\boldsymbol{x}_{\mu,\alpha}\|$ depends on α for certain regularization matrices. This kind of regularization matrices have been investigated and applied in [22].

PROPOSITION 2.2. *Assume that* (2.4) *holds and let* $\boldsymbol{x}_{\mu,\alpha}$ *denote the solution of* (2.3). *Let* A *be scaled so that* (1.10) *holds and assume that the regularization matrix* L *satisfies* $L^TL = VDV^T$, *where* V *is defined by the SVD of* A (1.9) *and* D *is a diagonal matrix. Then, for fixed* $\mu > 0$,

$$\frac{\partial}{\partial\alpha}\|\boldsymbol{x}_{\mu,\alpha}\|_2 \leq 0.$$

Proof. The requirement (2.4) and the fact that $\mu > 0$ secures that the solution $\boldsymbol{x}_{\mu,\alpha}$ exists and is unique; see the proof of Proposition 2.1. The normal equations (2.7) can be written as

$$\left(\mathrm{diag}[\sigma_1^{\alpha+1},\ldots,\sigma_r^{\alpha+1},0,\ldots,0] + \mu V^TL^TLV\right)\boldsymbol{y} = \mathrm{diag}[\sigma_1^{\alpha},\ldots,\sigma_r^{\alpha},0,\ldots,0](U^T\boldsymbol{b})_{1:n},$$

where $\boldsymbol{y} = [y_1, y_2, \ldots, y_n]^T = V^T\boldsymbol{x}$. Let

$$D = \mathrm{diag}[d_1, d_2, \ldots, d_n] = V^TL^TLV.$$

Due to the semidefiniteness of D and (2.4), we have $d_i \geq 0$ for $1 \leq i \leq r$ and $d_i > 0$ for $r < i \leq n$. Introduce the vector

$$\widetilde{\boldsymbol{b}} = [\widetilde{b}_1, \widetilde{b}_2, \ldots, \widetilde{b}_n]^T = (U^T\boldsymbol{b})_{1:n}.$$

Then

$$y_i = \begin{cases} \dfrac{\sigma_i^{\alpha}\widetilde{b}_i}{\sigma_i^{\alpha+1} + \mu d_i}, & 1 \leq i \leq r, \\ 0, & r < i \leq n. \end{cases}$$

It follows that

$$\frac{\partial}{\partial\alpha}\|\boldsymbol{y}\|_2^2 = 2\sum_{i=1}^{r}\frac{\sigma_i^{2\alpha}\ln(\sigma_i)\widetilde{b}_i^2\mu d_i}{(\sigma_i^{\alpha+1} + \mu d_i)^3} \leq 0$$

since $0 < \sigma_i < 1$ for all i. This shows the proposition. ∎

COROLLARY 2.3. *Assume that the conditions of Proposition 2.2 hold. Let* $\boldsymbol{x}_{\mu,\alpha}$ *solve* (2.3) *for some* $0 < \alpha \leq 1$ *and* $\mu > 0$. *Then* $d\mu_\alpha/d\alpha \geq 0$.

Proof. The result follows by combining the signs of $\partial\|\boldsymbol{x}_{\mu,\alpha}\|^2/\partial\alpha$ and $\partial\|\boldsymbol{x}_{\mu,\alpha}\|^2/\partial\mu$ shown in Propositions 2.1 and 2.2. ∎

3. Computation with fractional Tikhonov regularization. We first discuss the solution of minimization problems (1.14) of small to medium size. The solution of large-scale problems is considered below. For small to medium-sized problems, we apply the SVD of A to transform the minimization problem (1.14) to an equivalent problem in which the seminorm $\|\cdot\|_W$ of the fidelity term is replaced by the Euclidean norm. This allows us to apply already available methods for solving (1.14).

PROPOSITION 3.1. *Let the matrix A have the singular value decomposition* (1.9). *Introduce*

$$M = V\widetilde{S}_2^{(\alpha+1)/2}V^T, \qquad \boldsymbol{g} = V\widetilde{S}_1^{(\alpha-1)/2}U^T\boldsymbol{b},$$

where, for $\gamma \in \mathbb{R}$, we define

$$\widetilde{S}_2^{\gamma} = \mathrm{diag}[\sigma_1^{\gamma}, \sigma_2^{\gamma}, \ldots, \sigma_r^{\gamma}, 0, \ldots, 0] \in \mathbb{R}^{n\times n}$$

and the matrix $\widetilde{S}_1^{\gamma}$ is defined similarly as $\widetilde{S}_1^{\alpha}$ in (1.11). *Let the parameter $\alpha \geq 0$ be the same as in* (1.6). *Then*

$$\|A\boldsymbol{x} - \boldsymbol{b}\|_W = \|M\boldsymbol{x} - \boldsymbol{g}\|_2, \qquad \boldsymbol{x} \in \mathbb{R}^n. \tag{3.1}$$

Proof. We have

$$\|A\boldsymbol{x} - \boldsymbol{b}\|_W^2 = \boldsymbol{x}^T A^T W A\boldsymbol{x} - 2\boldsymbol{x}^T A^T W\boldsymbol{b} + \boldsymbol{b}^T W\boldsymbol{b}$$

and observe that

$$A^T W A = M^2, \qquad A^T W\boldsymbol{b} = M\boldsymbol{g}, \qquad \boldsymbol{b}^T W\boldsymbol{b} = \boldsymbol{g}^T\boldsymbol{g}.$$

This shows (3.1). □

Thus, instead of solving (1.14), we may solve

$$\min_{\boldsymbol{x}\in\mathbb{R}^n} \{\|M\boldsymbol{x} - \boldsymbol{g}\|_2^2 + \mu \|\boldsymbol{x}\|_{\mathrm{TV}}\}. \tag{3.2}$$

A variety of methods and software are available for solving this minimization problem. In the computed examples described in Section 4, we use the method described by Wen and Chan [25]. When, instead, the penalty term in (1.6) is replaced by the term (1.15) for some $0 < q < 2$, we apply the method described in [17] to solve the equivalent ℓ_2-ℓ_q problem

$$\min_{\boldsymbol{x}\in\mathbb{R}^n} \{\|M\boldsymbol{x} - \boldsymbol{g}\|_2^2 + \mu \|D\boldsymbol{x}\|_q^q\}. \tag{3.3}$$

The method in [17] also can be applied to solve (3.2). This method determines a sequence of approximate solutions in nested subspaces using the iteratively reweighted norm method described in [24], and replaces the penalty terms in (3.2) and (3.3) by weighted Euclidean norms, in which a diagonal weighting matrix is updated until a solution of (3.2) or (3.3) has been determined. The subspaces are generalized Krylov subspaces made up of the span of the residual vectors of the normal equations for each weighting matrix; see [17] for details.

We remark that the minimization problem (3.3) also can be solved by other methods, such as ADMM and proximal methods. Since the focus of the present paper is to study the advantage of combining the fractional Tikhonov method with a non-linear regularization term, a careful comparison of solution methods for (3.3) is outside the scope of this investigation. Comparisons of generalized Krylov subspace methods with the IRN method by Rodríguez and Wohlberg [24] are presented in [14, 17].

The transformation (3.1) followed by the solution of (3.2) is feasible when the matrix A is small enough to compute its SVD (1.9), or when A is large and has a

structure that makes it possible to determine its SVD for a reasonable cost. The latter situation arises, for instance, when A is the Kronecker product of two small to moderately-sized matrices. Discrete ill-posed problems with a matrix A with this structure arise in a variety of applications, including image restoration; see [4, 5] and references therein.

We turn to the situation when A is large and does not have a structure that can be exploited to compute its SVD in reasonable time. Then we first reduce the original problem (1.1) by a Krylov subspace method to obtain a problem of small to medium size to which the transformation (3.1) can be applied. For instance, application of ℓ steps of Golub–Kahan bidiagonalization to A with initial vector $\boldsymbol{b}$ gives the decompositions

$$AV_\ell = U_{\ell+1}\bar{C}_\ell, \qquad A^T U_\ell = V_\ell C_\ell^T, \qquad U_{\ell+1}\boldsymbol{e}_1 = \boldsymbol{b}/\|\boldsymbol{b}\|_2, \tag{3.4}$$

where the matrices $U_{\ell+1} \in \mathbb{R}^{m\times(\ell+1)}$ and $V_\ell \in \mathbb{R}^{n\times\ell}$ have orthonormal columns, and the lower bidiagonal matrix $\bar{C}_\ell \in \mathbb{R}^{(\ell+1)\times\ell}$ has positive diagonal and subdiagonal entries. Moreover, $U_\ell \in \mathbb{R}^{m\times\ell}$ is made up of the ℓ first columns of $U_{\ell+1}$, $C_\ell \in \mathbb{R}^{\ell\times\ell}$ consists of the first ℓ rows of $\bar{C}_\ell$, and $\boldsymbol{e}_1 = [1, 0, \ldots, 0]^T$ denotes the first axis vector. The columns of V_ℓ span the Krylov subspace

$$\mathcal{K}_\ell(A^TA,\, A^T\boldsymbol{b}) = \text{span}\{A^T\boldsymbol{b},\, (A^TA)A^T\boldsymbol{b},\, \ldots,\, (A^TA)^{\ell-1}A^T\boldsymbol{b}\};$$

see, e.g., [3, 9] for details. The number of bidiagonalization steps, ℓ, generally can be chosen fairly small. We assume ℓ to be small enough so that no breakdown occurs. The occurrence of breakdown is rare and simplifies the computations.

It follows from (3.4) that

$$\min_{\boldsymbol{x}\in\mathcal{K}_\ell(A^TA,A^T\boldsymbol{b})} \|A\boldsymbol{x}-\boldsymbol{b}\|_2 = \min_{\boldsymbol{y}\in\mathbb{R}^\ell} \|\bar{C}_\ell\boldsymbol{y} - \boldsymbol{e}_1\|\boldsymbol{b}\|_2\,\|_2. \tag{3.5}$$

Thus, application of ℓ steps of Golub–Kahan bidiagonalization reduces a large minimization problem (1.1) to the small minimization problem in the right-hand of (3.5). Instead of solving the minimization problem (1.14) with a large matrix A, we solve the reduced problem

$$\min_{\boldsymbol{y}\in\mathbb{R}^\ell} \{\|\bar{C}_\ell\boldsymbol{y} - \boldsymbol{e}_1\|\boldsymbol{b}\|_2\,\|_W^2 + \mu\,\|V_\ell\boldsymbol{y}\|_{\mathrm{TV}}\}.$$

The transformation (3.1) can be applied to the small matrix $\bar{C}_\ell$.

We remark that reduction methods different from Golub–Kahan bidiagonalization can be applied to reduce a large-scale problem to a small or moderately sized problem, such as methods based on the Arnoldi process. A recent overview of reduction and regularization methods for linear discrete ill-posed problems is presented by Gazzola et al. [7].

4. Computed examples. This section presents numerical results that illustrate the performance of the proposed fractional Tikhonov regularization methods (3.2) and (3.3) with a TV-norm or ℓ_q-norm regularizer. We refer to the method (3.2) as Frac-TV and to the method (3.3) as Frac-ℓ_q in the figures and tables. For all examples, we set $q = 0.6$ in (3.3). These fractional Tikhonov methods are compared to standard Tikhonov regularization (1.4) (denoted by ℓ_2-Tik), the method

$$\min_{\boldsymbol{x}\in\mathbb{R}^n} \{\|A\boldsymbol{x}-\boldsymbol{b}\|_2^2 + \mu\,\|\boldsymbol{x}\|_{\mathrm{TV}}\},$$

which we refer to as ℓ_2-TV, as well as to the method (1.6), which is denoted by Frac-Tik. These methods are applied to the restoration of signals in one space-dimension and images in two space-dimensions. The available signals are contaminated by white Gaussian noise and Gaussian blur. The quality of the restorations computed with the various methods is for signals in one space-dimension measured by the relative error norm

$$\mathrm{e}(\boldsymbol{x}^*, \widehat{\boldsymbol{x}}) := \frac{\|\boldsymbol{x}^* - \widehat{\boldsymbol{x}}\|_2}{\|\widehat{\boldsymbol{x}}\|_2},$$

where $\boldsymbol{x}^*$ denotes the computed approximation of the desired signal $\widehat{\boldsymbol{x}}$. For image restoration problems, we compute the Signal-to-Noise Ratio (SNR), which is defined as

$$\mathrm{SNR}(\boldsymbol{x}^*, \widehat{\boldsymbol{x}}) := 10 \log_{10} \frac{\|\widehat{\boldsymbol{x}} - E(\widehat{\boldsymbol{x}})\|_2^2}{\|\boldsymbol{x}^* - \widehat{\boldsymbol{x}}\|_2^2}, \tag{4.1}$$

where $E(\widehat{\boldsymbol{x}})$ denotes the mean gray level of $\widehat{\boldsymbol{x}}$. We tabulate the Improved Signal-to-Noise Ratio (ISNR),

$$\mathrm{ISNR}(\boldsymbol{x}^*, \widehat{\boldsymbol{x}}, \boldsymbol{b}) := \mathrm{SNR}(\boldsymbol{x}^*, \widehat{\boldsymbol{x}}) - \mathrm{SNR}(\boldsymbol{b}, \widehat{\boldsymbol{x}}),$$

where the vector $\boldsymbol{b}$ represents the available blur- and noise-contaminated image. The ISNR-value provides a quantitative measure of the improvement in the quality of the restored image; a large ISNR-value indicates that the computed restoration $\boldsymbol{x}^*$ is an accurate approximation of the desired blur- and noise-free signal $\widehat{\boldsymbol{x}}$ relative to $\boldsymbol{b}$.

The relative noise contamination is measured by the noise level

$$\varepsilon := \frac{\delta}{\|\widehat{\boldsymbol{x}}\|},$$

where δ bounds the error $\boldsymbol{e}$ in $\boldsymbol{b}$; see (1.2) and (2.1). In all examples the inequality (2.1) is sharp. All computations were carried out in MATLAB with about 15 significant decimal digits.

Example 4.1. This example illustrates the performance of the restoration methods when applied to several signals in one space-dimension. Each signal has $n = 200$ equidistant samples. We consider a piece-wise constant signal, referred to as `signal`, a signal with sharp jumps, denoted `bumps`, and a smooth signal, referred to as `shaw`. The latter signal is generated with the function `shaw` from [11]. The signals `signal` and `bumps` are corrupted by Gaussian blur and white Gaussian noise. The blur is generated by the function

$$G(t) = \frac{1}{\sqrt{2\pi\sigma^2}} \exp\left(-\frac{t^2}{2\sigma^2}\right). \tag{4.2}$$

The parameter σ, referred to as `sigma` below, is the standard deviation of the Gaussian distribution. Larger `sigma`-values give more blur. Equidistant sampling of G determines a symmetric Toeplitz matrix $T \in \mathbb{R}^{200\times 200}$. We set the smallest elements to zero, i.e., we approximate T by a symmetric banded Toeplitz matrix with bandwidth `band`. This defines the blurring matrix A used in this example. Our blurring matrix is an analogue for one space-dimension of the blurring matrix determined by the function `blur` from [11] that approximates blur in two space-dimensions.

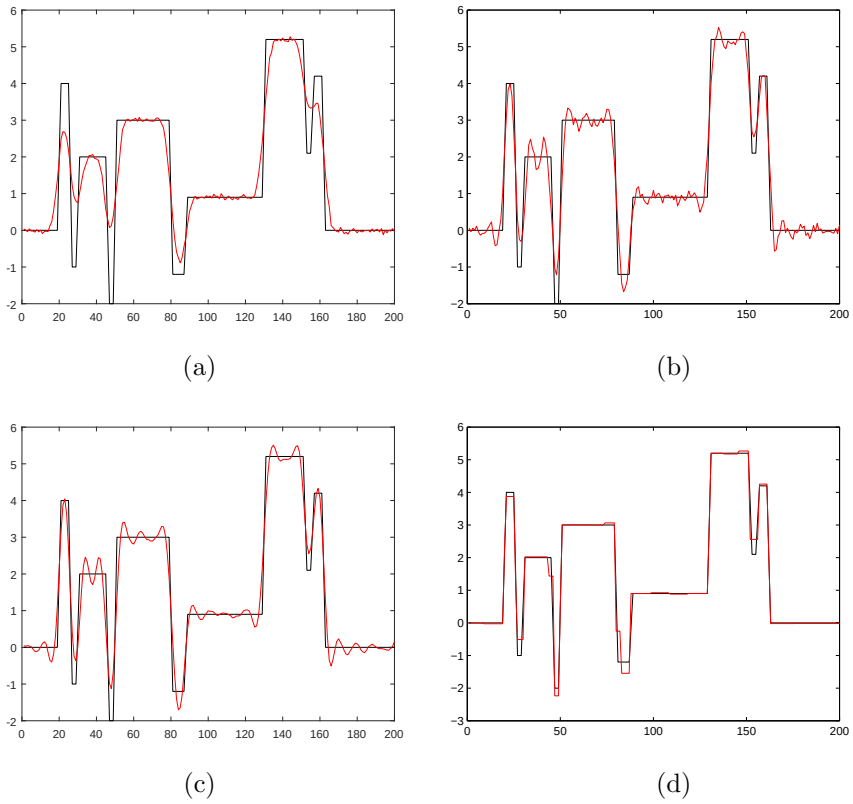

FIG. 4.1. *Example 4.1. All figures show the desired blur- and noise-free signal* $\widehat{\boldsymbol{x}}$ *(in black). The given contaminated signal* $\boldsymbol{b}$ *is shown in figure (a). Contamination is by Gaussian blur with parameters* `sigma`*=3 and* `band`*=11, and white Gaussian noise of noise level* 0.02*. The remaining figures display restorations computed by Frac-Tik (b), Frac-TV (c), and Frac-*ℓ_q *(d).*

Our first illustrations show restorations of contaminations of the piece-wise constant signal `signal`. The blurring matrix A is defined as described above with parameters `sigma`=3, and `band`=11. White Gaussian noise corresponding to the noise level 0.02 is added to the blurred signal; cf. (1.2). This defines the contaminated signal that we would like to restore.

Figure 4.1 displays the exact, the contaminated, and restored signals `signal`. The Frac-ℓ_q method is seen to deliver the most accurate restoration. Relative errors of the restorations of the figure are shown in the second line of results of Table 4.1. The entries XeY of the tables stand for $\mathrm{X}\cdot 10^{\mathrm{Y}}$. The value $\alpha = 0.1$ is used for the fractional methods; see (1.6) and (1.7). The table also displays results for other methods, blurs, and noise levels ε, and for another α-value. The smallest relative errors are depicted in boldface. The Frac-TV method is seen to be competitive with all methods except for Frac-ℓ_q. We remark that the ℓ_2-TV method is known to generally perform well when restoring piece-wise constant signals. Table 4.1 shows both the Frac-TV and Frac-ℓ_q methods to give more accurate restorations than the ℓ_2-TV method. The Frac-TV method is implemented with an algorithm based on a variant of the proximal primal-dual method described in [25], which applies the discrepancy principle to choose the regularization parameter. Finally, the Frac-ℓ_q and ℓ_2-ℓ_q methods are

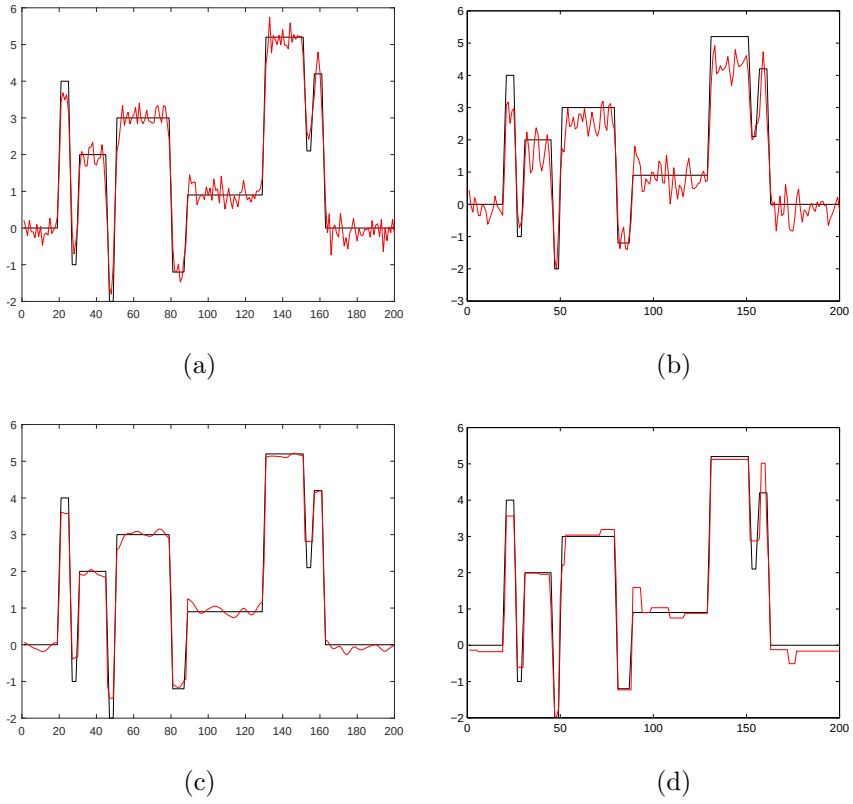

FIG. 4.2. *Example 4.1. All figures show the desired blur- and noise-free signal* $\widehat{\boldsymbol{x}}$ *(in black). The given contaminated signal* $\boldsymbol{b}$ *is shown in figure (a). Contamination is by Gaussian blur with parameters* `sigma`*=1 and* `band`*=5, and white Gaussian noise of noise level* 0.1*. The remaining figures display restorations computed by Frac-Tik (b), Frac-TV (c), and Frac-*ℓ_q *(d).*

implemented following the approach suggested in [17]. Differently from the ℓ_2-TV and Frac-TV methods, the Frac-ℓ_q and ℓ_2-ℓ_q methods require the solution of a sequence of minimization problems (3.3) for different μ-values to determine a value such that the computed solution satisfies the discrepancy principle.

Figure 4.2 is analogous to Figure 4.1. It differs from the latter only in that the signal `signal` to be restored as been contaminated by more white Gaussian noise and less blur. Similarly as in Figure 4.1, the fractional methods Frac-TV and Frac-ℓ_q deliver the most accurate restorations.

Table 4.2 displays the relative error in restorations of a contaminated version of the signal `signal` by the fractional methods Frac-Tik, Frac-TV, and Frac-ℓ_q for different α-values; see (1.6) and (1.7). For all α-values, Frac-TV gives better restorations than Frac-Tik, and the most accurate approximations of $\widehat{\boldsymbol{x}}$ are delivered by Frac-ℓ_q. All α-values in the interval $[0.01, 0.3]$ give improvements in the restorations, when compared with restorations determined by ℓ_2-Tik. This fact and the table illustrate that the choice of the α-value in (1.6) and (1.7) is not critical.

Results for the signal `shaw` are displayed in Figure 4.3 as well as by Table 4.3. The Frac-ℓ_q method gives superior restorations. Since the signal `shaw` is smooth, methods that use the TV-norm, i.e., ℓ_2-TV and Frac-TV, do not perform very well.

Gaussian blur with parameters `sigma`=1 and `band`=5 ($\alpha = 0.1$)

ε	ℓ_2-Tik	Frac-Tik	ℓ_2-TV	Frac-TV	ℓ_2-ℓ_q	Frac-ℓ_q
0.01	4.1931e-02	4.2179e-02	4.9024e-02	4.3679e-02	1.8071e-02	**1.6618e-02**
0.02	5.8877e-02	6.6635e-02	6.3192e-02	2.5697e-02	2.6278e-02	**2.3555e-02**
0.10	1.4787e-01	1.6069e-01	1.2932e-01	9.8602e-02	9.7290e-02	**9.3078e-02**

Gaussian blur with parameters `sigma`=2 and `band`=5 ($\alpha = 0.1$)

ε	ℓ_2-Tik	Frac-Tik	ℓ_2-TV	Frac-TV	ℓ_2-ℓ_q	Frac-ℓ_q
0.01	7.3733e-02	7.5839e-02	8.0086e-02	2.8287e-02	1.2721e-02	**1.2524e-02**
0.02	9.5036e-02	1.0035e-01	9.7589e-02	5.0231e-02	4.6128e-02	**4.4535e-02**
0.10	1.7461e-01	1.9253e-01	1.5257e-01	**1.1815e-01**	1.2521e-01	1.2492e-01

Gaussian blur with parameters `sigma`=3 and `band`=11 ($\alpha = 0.01$)

ε	ℓ_2-Tik	Frac-Tik	ℓ_2-TV	Frac-TV	ℓ_2-ℓ_q	Frac-ℓ_q
0.01	1.5396e-01	1.5361e-01	1.5829e-01	1.5747e-01	9.5329e-02	**7.7923e-02**
0.02	1.6990e-01	1.6993e-01	1.7359e-01	1.7266e-01	1.0761e-01	**1.0105e-01**
0.10	2.2669e-01	2.2683e-01	2.5229e-01	2.5064e-01	1.7761e-01	**1.0116e-01**

TABLE 4.1

Example 4.1. Relative errors in the restoration of blur- and noise-contaminated signals `signal`. *Results for different Gaussian blurs, defined by the parameters* `sigma` *and* `band`, *for three noise levels are shown.*

α	Frac-Tik	Frac-TV	Frac-ℓ_q
0.01	2.4102e-01	2.0830e-01	**1.5898e-01**
0.05	2.4472e-01	2.0637e-01	**1.5315e-01**
0.10	2.5082e-01	2.0331e-01	**1.4845e-01**
0.20	2.7090e-01	1.6231e-01	**1.3469e-01**
0.30	3.1165e-01	1.5968e-01	**1.4265e-01**

TABLE 4.2

Example 4.1. Relative errors in the restored of corrupted version of the signal `signal`. *Contamination is by Gaussian blur with parameters* `sigma`*=1 and* `band`*=5 and by additive zero-mean white Gaussian noise with noise level* $\varepsilon = 0.2$. *The restorations are determined with fractional methods for different* α*-values.*

The signal `bumps`, a corrupted version, as well as restorations are displayed by Figure 4.4. Table 4.4 displays quantitative results for two noise levels. The signal `bumps` is "rough" and Frac-TV and Frac-ℓ_q give more accurate restorations than the other methods in our comparison. □

Example 4.2. This example is concerned with image restoration. We compare the proposed fractional Tikhonov regularization method Frac-TV to the ℓ_2-TV method for the restoration of images corrupted by white Gaussian noise and Gaussian blur. The fractional parameter for Frac-TV is $\alpha = 0.02$. Both the Frac-TV and ℓ_2-TV restoration methods determine the regularization parameter μ by the discrepancy principle in each iteration step. The iterations are terminated when the relative

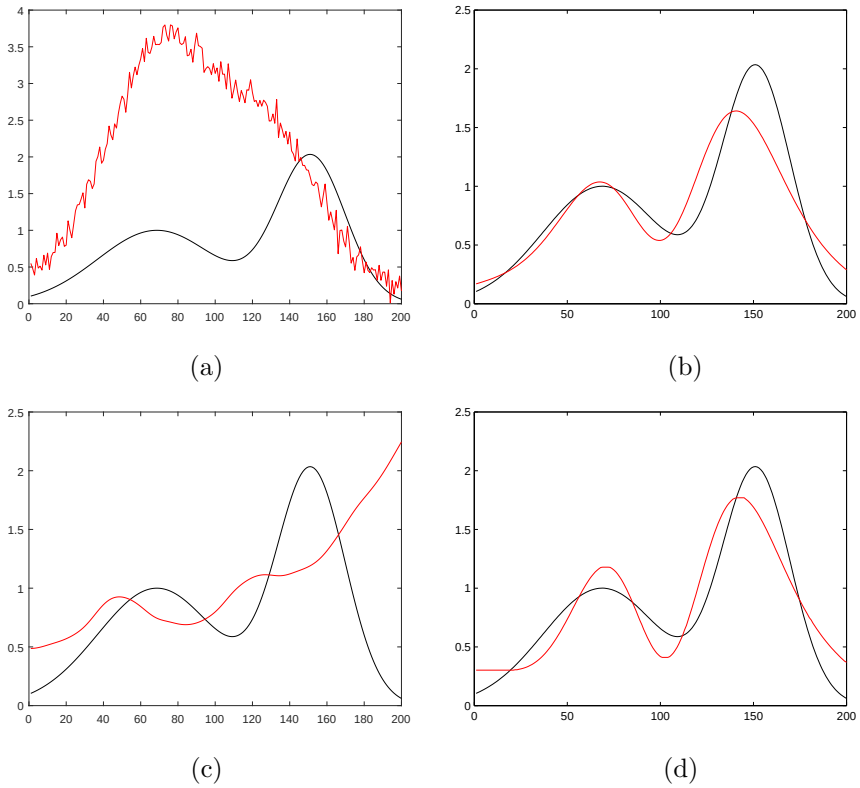

FIG. 4.3. *Example 4.1. All figures show the desired blur- and noise-free signal* `shaw` *(in black). The given contaminated signal* $\boldsymbol{b}$ *is shown in figure (a). Contamination is by Gaussian blur with parameters* `sigma=1` *and* `band=5`*, and white Gaussian noise of noise level* 0.05*. The remaining figures display restorations computed by Frac-Tik (b), Frac-TV (c), and Frac-*ℓ_q *(d).*

ε	ℓ_2-Tik	Frac-Tik	ℓ_2-TV	Frac-TV	ℓ_2-ℓ_q	Frac-ℓ_q
0.01	1.5415e-01	1.5349e-01	2.3594e-01	2.3509e-01	1.4528e-01	**1.4352e-01**
0.05	1.9258e-01	1.9283e-01	6.8813e-01	6.7791e-01	1.8618e-01	**1.6801e-01**

TABLE 4.3

Example 4.1. Relative errors in restorations of contaminated `shaw` *signals. Noise contamination is given by additive zero-mean white Gaussian noise with noise level* ε*. The fractional parameter is* $\alpha = 0.01$.

difference between successive iterates $\boldsymbol{x}^{(k)}$ is small enough, i.e., as soon as

$$\|\boldsymbol{x}^{(k)} - \boldsymbol{x}^{(k-1)}\|_2 \;/\; \|\boldsymbol{x}^{(k-1)}\|_2 < 2 \cdot 10^{-3}.$$

The restoration methods are applied to the test image `checkerboard` shown in Figure 4.5(a), which is corrupted by Gaussian blur and additive white Gaussian noise. The blur is defined by a Gaussian function in two space-dimension, analogous to (4.2). We measure the performance of the Frac-TV and ℓ_2-TV methods in terms of the ISNR-values of the restored images for several noise levels ε. Results are displayed in Table 4.5. The quality of the corrupted image of Figure 4.5(a) is measured by the Signal-to-Noise ratio (4.1). We denote this quantity by SNR_0 in Table 4.5. The

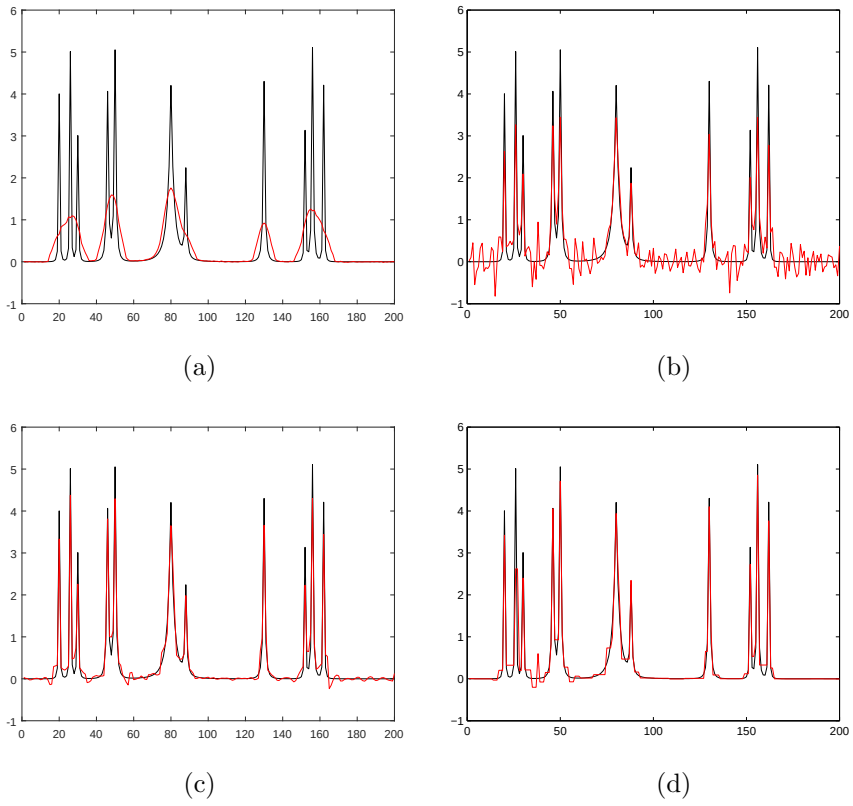

FIG. 4.4. *Example 4.1. All figures show the desired blur- and noise-free signal* `bumps` *(in black). The given contaminated signal* $\boldsymbol{b}$ *is shown in figure (a). Contamination is by Gaussian blur with parameters* `sigma`*=3 and* `band`*=11, and white Gaussian noise of noise level* 0.01*. The remaining figures display restorations computed by Frac-Tik (b), Frac-TV (c), and Frac-*ℓ_q *(d).*

ε	ℓ_2-Tik	Frac-Tik	ℓ_2-TV	Frac-TV	ℓ_2-ℓ_q	Frac-ℓ_q
0.01	4.0679e-01	4.0012e-01	2.1345e-01	1.9524e-01	1.3333e-01	**1.1915e-01**
0.05	6.8008e-01	6.7703e-01	6.9673e-01	6.9721e-01	6.9310e-01	**6.4459e-01**

TABLE 4.4

Example 4.1. Relative errors in restorations of contaminated `bumps` *signals. Contamination is by Gaussian blur with parameters* `sigma`*=3 and* `band`*=5, and additive zero-mean white Gaussian noise with noise level* ε*. The fractional parameter is* $\alpha = 0.01$.

table shows Frac-TV to determine a restoration of higher quality than ℓ_2-TV. We use TV-norm regularization because this kind of regularization is known to perform well for "blocky" images. The restorations of the contaminated image of Figure 4.5(a) determined by ℓ_2-TV and Fract-TV are depicted by Figure 4.5(b) and Figure 4.5(c), respectively. □

5. Conclusions. Fractional regularization methods have recently received considerable attention. This paper describes how the use of a fractional fidelity term can be combined with a TV-norm or ℓ_q-quasi-norm regularization term with $0 < q < 1$. Computed examples illustrate that the fractional regularization methods so defined

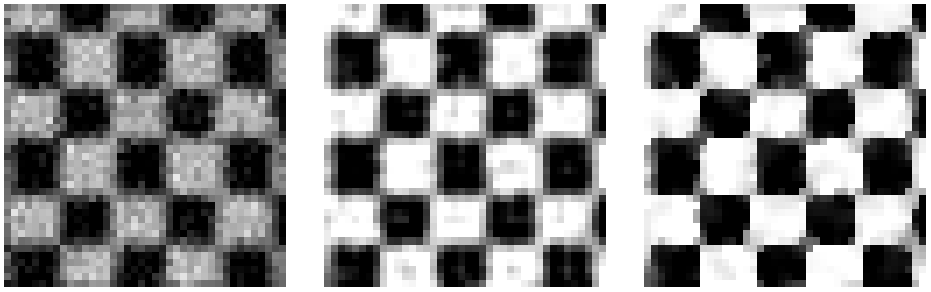

(a) (b) (c)

FIG. 4.5. *Example 4.2. Restoration of the* `checkerboard` *image: corrupted image contaminated by Gaussian blur with parameters* `sigma`*=1.1 and* `band`*=3, and by white Gaussian noise of noise level* 0.2*, SNR = 3.5703 (a), restoration computed by ℓ_2-TV, ISNR = 4.26 (b), and restoration computed by Frac-TV, ISNR = 6.23 (c).*

ε	SNR_0	ℓ_2-TV	Frac-TV
0.1	3.67	5.36	9.19
0.2	3.42	4.26	6.23
0.3	3.19	3.71	4.96

TABLE 4.5

Example 4.2. ISNR values for restorations of contaminated `checkerboard` *image. Contamination is by Gaussian blur with parameters* `sigma`*=1.1 and* `band`*=3, and additive zero-mean white Gaussian noise with noise level ε.*

may determine restorations of signals in one or two space-dimensions of higher quality than restorations obtained when the size of the regularization term is measured by the Euclidean vector norm.

Acknowledgements. This work was supported by the "National Group for Scientific Computation (GNCS-INDAM)" and by ex60% project by the University of Bologna "Funds for selected research topics".

REFERENCES

[1] Z. Bai, The CSD, GSVD, their applications and computation, IMA preprint 958, Institute for Mathematics and its Applications, University of Minnesota, Minneapolis, MN, 1992.
[2] D. Bianchi, A. Buccini, M. Donatelli, and S. Serra–Capizzano, Iterated fractional Tikhonov regularization, Inverse Problems, 31 (2015), 055005.
[3] Å. Björck, Numerical Methods in Matrix Computations, Springer, New York, 2015.
[4] A. Bouhamidi and K. Jbilou, Sylvester Tikhonov-regularization methods in image restoration, J. Comput. Appl. Math., 206 (2007), pp. 86–98.
[5] A. Bouhamidi, K. Jbilou, L. Reichel, and H. Sadok, An extrapolated TSVD method for linear discrete ill-posed problems with Kronecker structure, Linear Algebra Appl., 434 (2011), pp. 1677–1688.
[6] X. Chen, M.K. Ng, and C. Zhang, Non-Lipschitz ℓ_p-regularization and box constrained model for image restoration, IEEE Trans. Image Processing, 21 (2012), pp. 4709–4721.
[7] S. Gazzola, P. Novati, and M. R. Russo, On Krylov projection methods and Tikhonov regularization, Electron. Trans. Numer. Anal., 44 (2015), pp. 83–123.
[8] D. Gerth, E. Klann, R. Ramlau, and L. Reichel, On fractional Tikhonov regularization, J. Inverse Ill-Posed Probl., 23 (2015), pp. 611–625.
[9] G. H. Golub and C. F. Van Loan, Matrix Computations, 4th ed., Johns Hopkins University Press, Baltimore, 2013.

[10] P. C. Hansen, Rank-Deficient and Discrete Ill-Posed Problems, SIAM, Philadelphia, 1998.
[11] P. C. Hansen, Regularization tools version 4.0 for Matlab 7.3, Numer. Algorithms, 46 (2007), pp. 189–194.
[12] M. E. Hochstenbach, S. Noschese, and L. Reichel, Fractional regularization matrices for linear discrete ill-posed problems, J. Eng. Math., 93 (2015), pp. 113–129.
[13] M. E. Hochstenbach and L. Reichel, Fractional Tikhonov regularization for linear discrete ill-posed problems, BIT, 51 (2011), pp. 197–215.
[14] G. Huang, A. Lanza, S. Morigi, L. Reichel, and F. Sgallari, Majorization-minimization generalized Krylov subspace methods for ℓ_p-ℓ_q optimization applied to image restoration, BIT, in press.
[15] S. Kindermann, Convergence analysis of minimization-based noise level-free parameter choice rules for linear ill-posed problems, Electron. Trans. Numer. Anal., 38 (2011), pp. 233–257.
[16] E. Klann and R. Ramlau, Regularization by fractional filter methods and data smoothing, Inverse Problems, 24 (2008), 025018.
[17] A. Lanza, S. Morigi, L. Reichel, and F. Sgallari, A generalized Krylov subspace method for ℓ_p-ℓ_q minimization, SIAM J. Sci. Comput., 37 (2015), pp. S30–S50.
[18] A. Lanza, S. Morigi, F. Sgallari, Constrained TVp-L2 model for image restoration, J. Scientific Computing, 68 (2016), pp. 64–91.
[19] A. K. Louis, Inverse und schlecht gestellte Probleme, Teubner, Stuttgart, 1989.
[20] P. Mathé and U. Tautenhahn, Enhancing linear regularization to treat large noise, J. Inverse Ill-Posed Problems, 19 (2011), pp. 859–879.
[21] S. Noschese and L. Reichel, Lavrentiev-type regularization methods for Hermitian problems, Calcolo, 52 (2015), pp. 187–205.
[22] S. Noschese and L. Reichel, Some matrix nearness problems suggested by Tikhonov regularization, Linear Algebra Appl., 502 (2016), pp. 366–386.
[23] L. Reichel and G. Rodriguez, Old and new parameter choice rules for discrete ill-posed problems, Numer. Algorithms, 63 (2013), pp. 65–87.
[24] P. Rodríguez and B. Wohlberg, Efficient minimization method for a generalized total variation functional, IEEE Trans. Image Process., 18 (2009), pp. 322–332.
[25] Y. W. Wen and R. H. Chan, Parameter selection for total variation based image restoration using discrepancy principle, IEEE Trans. Image Process., 21 (2012), pp. 1770–1781.